View Article Online
View Journal

Dalton Transactions

An international journal of inorganic chemistry

Accepted Manuscript

This article can be cited before page numbers have been issued, to do this please use: M. Gallardo-Villagrán, O. Rivada-Wheelaghan, W. Rahaman, R. R. Fayzullin and J. R. Khusnutdinova, *Dalton Trans.*, 2020, DOI: 10.1039/D0DT02505D.

ROYAL SOCIETY OF CHEMISTRY

rsc.li/dalton

View Article Online
DOI: 10.1039/D0DT02505D

ARTICLE

Proton-responsive naphthyridinone-based Ru^{II} complexes and their reactivity with water and alcohols

Received 00th January 20xx,
Accepted 00th January 20xx

DOI: 10.1039/x0xx00000x

Manuel Gallardo-Villagrán,[a,§] Orestes Rivada-Wheelaghan,[a,†,§] S. M. Wahidur Rahaman,[a] Robert R. Fayzullin,[b] Julia R. Khusnutdinova*[a]

We report the synthesis and reactivity of Ru^{II} complexes with a new naphthyridinone-substituted phosphine ligand, 7-(diisopropylphosphinomethyl)-1,8-naphthyridin-2(1H)-one (**L-H**), which contains two reactive sites that can potentially be deprotonated by a strong base: an NH proton of naphthyridinone and a methylene arm attached to the phosphine. In the absence of a base, the stable bis-ligated complex Ru(**L-H**)$_2$Cl$_2$ (**1**) containing two NH groups in the secondary coordination sphere, is formed. Upon further reaction with a base, a doubly deprotonated, dimeric complex is obtained [Ru$_2$(**L*-H**)$_2$(**L**)$_2$] (**2**), in which two of four ligands undergo deprotonation at the NH (**L**), while the other two ligands are deprotonated at the methylene groups (**L*-H**) as confirmed by an X-ray diffraction study; intramolecular hydrogen bonding is present between the NH group of one ligand and an O-atom of another ligand in the dimeric structure, which stabilizes the observed geometry of the complex. Complex **2** reacts with protic solvents such as water or methanol generating aqua Ru(**L**)$_2$(OH$_2$)$_2$ (**3**) or methanol complexes Ru(**L**)$_2$(MeOH)$_2$ (**4**), respectively, both exhibiting intramolecular H-bonded patterns with surrounding ligands at least in the solid state. These complexes react with benzyl alcohols to give aldehydes via base-free acceptorless dehydrogenation.

Introduction

Development of ligands that can act not only as spectators but also participate in proton transfer and/or bond activation in tandem with the metal center, attracts significant attention both in artificial catalysis and in biomimetic chemistry, where proton transfer is often conducted with help of the surrounding functional groups in the primary or secondary coordination spheres.[1-4] Ligands which can be deprotonated or can act as the proton shuttle groups have been shown to have great potential in the discovery of new types of bond activation, as well as in homogeneous or electrochemical catalysis that involves proton transfer and hydrogen generation/formation.[5-7] In particular, the location of proton responsive groups in the secondary coordination sphere (SCS) in proximity to the reactive metal center may result in cooperative effects, enabling the activation and/or functionalization of various substrates,[8-10] and catalytic performance.[11-13] A great variety of ligand motifs featuring reactive NH,[4, 14] OH[15-24] and CH groups [1-2, 25-27] have been developed over the past several decades by many research groups, and such ligands have been actively utilized to promote various types of catalytic or stoichiometric bond activation. Utilizing the SCS strategy, notable breakthroughs in the development of low-barrier processes involving hydrogen or proton transfer have been reported. Specifically, Szymczak *et al.* showed that addition of proton-switchable groups at the ligand framework induced new catalytic performance in ruthenium complexes, revealing the crucial role pendant hydroxyl groups can play in catalytic activity.[12, 28] More recently, Achard *et al.* reported a set of Ru complexes bearing proton responsive pyridonate motifs to perform catalytic ester formation and cross-coupling of alcohols to form α-alkylated ketones in the presence of a base.[29-30] We have recently shown that the presence of two hydroxy groups in proximity to a Mn center in substituted bipyridyl-derived complexes induced higher catalytic activity on CO_2 hydrogenation and transfer hydrogenation of carbonyl groups, imines and aromatic N-heterocycles.[31-32]

In our previous work, we utilized naphthyridinone framework attached to the various chelating ligand motifs, in particular, mono- and bis-picolylamines, to build multimetallic complexes.[33-34] These ligands were conveniently prepared through a chloromethyl-substituted common precursor, which

[a] *Coordination Chemistry and Catalysis Unit, Okinawa Institute of Science and Technology Graduate University 1919–1 Tancha, Onna–son, 904–0495, Okinawa, Japan. Email: juliak@oist.jp*
[b] *Arbuzov Institute of Organic and Physical Chemistry, Kazan Scientific Center, Russian Academy of Sciences, 8 Arbuzov Street, Kazan 420088, Russian Federation.*
† Current address: *Université de Paris, Laboratoire d'Electrochimie Moléculaire, UMR 7591 CNRS, 15 rue Jean-Antoine de Baïf, F-75205 Paris Cedex 13, France .*
Deposition numbers 2009670-2009673 contain the supplementary crystallographic data for this paper. These data are provided free of charge by the joint Cambridge Crystallographic Data Centre and Fachinformationszentrum Karlsruhe Access Structures service www.ccdc.cam.ac.uk/structures.
Electronic Supplementary Information (ESI) available: [details of any supplementary information available should be included here]. See DOI: 10.1039/x0xx00000x

shows great potential in further diversification of ligand motifs that can be obtained by varying a chelating fragment. In this work, we decided to design a new ligand that combines phosphinomethyl and naphthyridinone fragments and study the reactivity of its Ru complexes reactivity in deprotonation and in reactions with protic solvents. The ability of (phosphinomethyl)pyridine-derived ligands to undergo deprotonation at the acidic methylene arm, leading to N-heterocycle dearomatization, is well-precedented and has led to the discovery of a large class of acceptorless dehydrogenation and hydrogenation catalysts.[1-2, 25-26] The examples of the ligands that feature both acidic methylene arms and NH groups still remain relatively rare. For example, PNNH ligand showing dual reactivity mode was developed in the Milstein group and was utilized for metal-ligand cooperative bond activation and catalytic (de)hydrogenation reactions.[35-36] Van der Vlugt and co-workers reported Ru complexes with bipyridyl-based PNN(O) ligand active in acceptorless dehydrogenative coupling reactions.[37]

The new napthyridinone-based ligand developed in this work would potentially have two possible sites for deprotonation: an acidic CH_2 moiety attached to phosphine arm as well as the NH group of naphthyridinone. Furthermore, by using this ligand to support mononuclear complexes, we can explore the reactivity of the proton-responsive naphthyridinone group present in the SCS of the metal.

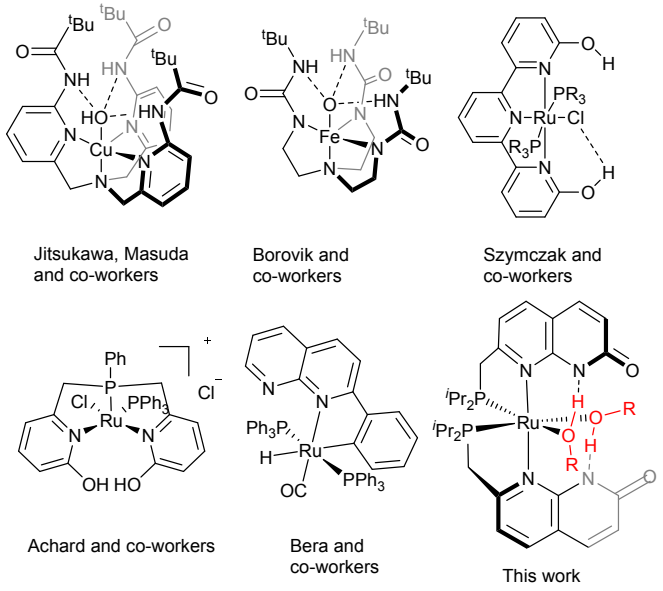

Fig 1. Representative examples of coordination complexes containing proton responsive groups in the secondary coordination sphere.

Results and discussion

Synthesis and characterization of ligand and Ru complexes

We have recently reported 7-(chloromethyl)-1,8-naphthyridin-2(1*H*)-one (*ClNaph*) as a precursor to develop multidentate donor ligands and generate multimetallic architectures.[33-34] To synthesize a proton-responsive naphthyridinone-substituted phosphine ligand, we reacted this precursor with $^{i}Pr_2PH$ in MeOH, followed by treatment with aqueous $NaHCO_3$ solution and extraction of the desired ligand **L-H** into dichloromethane. After drying over $MgSO_4$ and solvent removal, the desired ligand **L-H** was obtained in 63% yield (Scheme 1).

View Article Online DOI: 10.1039/D0DT02595D

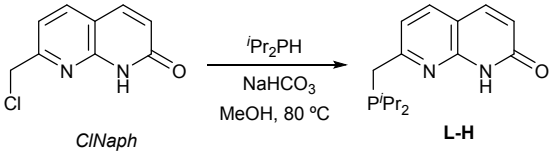

Scheme 1 Synthesis of ligand **L-H**.

Reaction of 1 equivalent of **L-H** with 0.49 equivalents of $[RuCl_2(DMSO)_4]$ at 80 °C for 8 hours in THF yielded an orange solid identified as the dichloride ruthenium complex [Ru(**L-H**)$_2$Cl$_2$] (**1**) (Scheme 2). The $^{31}P\{^{1}H\}$ NMR spectrum shows one singlet at 70.29 ppm in CD_3CN. In the ^{1}H NMR spectrum, a singlet of the N–H group is observed at 11.32 ppm in CD_2Cl_2 solution; two multiplets at 4.70 and 3.58 ppm have been assigned to the inequivalent geminal methylene protons of **L-H**.

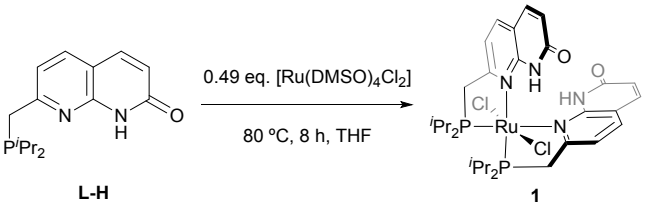

Scheme 2 Formation of complex **1**.

Single crystal X-ray diffraction (XRD) study of complex **1** reveals an octahedral geometry around Ru with two Cl-atoms located *trans* to each other, and phosphine atoms of **L-H** in *cis* orientation. The most characteristic feature of this structure (Fig. 2) is the presence of an intramolecular N–H···Cl hydrogen bond. These interactions could explain the downfield shift of the N–H proton peak in the ^{1}H NMR spectrum relative to the corresponding chemical shift in the free **L-H** ligand (10.23 ppm). The puckered five-membered chelate ring is consistent with inequivalent geminal methylene protons in the ^{1}H NMR spectrum, and the presence of N–H···Cl hydrogen bonds likely leads to the lack of conformational fluxionality.

View Article Online
DOI: 10.1039/D0DT02505D

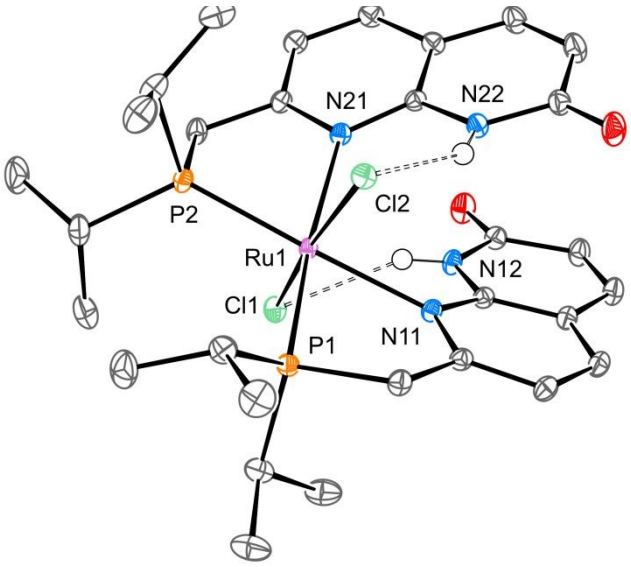

Fig. 2 ORTEP of **1** at 60 % probability level according to single crystal X-ray diffraction data. Solvent molecules and hydrogen atoms, except for N–H, are omitted for clarity. Selected interatomic distances [Å]: Ru1–N11 2.2303(8), Ru1–N21 2.2553(8), Ru1–P1 2.2849(2), Ru1–P2 2.2892(2), Ru1–Cl1 2.4321(2), Ru1–Cl2 2.4346(2). H-bond N12–H12···Cl1 [Å, °]: N12–H12 0.851(13), H12···Cl1 2.318(14), N12···Cl1 3.0937(8), ∠N12–H12···Cl1 151.6(14). H-bond N22–H22···Cl2 [Å, °]: N22–H22 0.854(13), H22···Cl2 2.387(14), N22···Cl2 3.1509(8), ∠N22–H22···Cl2 149.1(13).

Reactivity of 1 in the presence of bases

Considering the presence of two NH groups in complex **1**, we aimed to study its reactivity in the presence of bases, anticipating that a base could also assist in removing the Cl ligands and introduce a free coordination site for further reactivity. In addition, phosphinomethylene groups attached to naphthyridinone might potentially serve as another potential site of deprotonation.[2] No deprotonation was observed in the presence of weak carbonates bases. When **1** was reacted with 2.2 equiv. of ^{t}BuOK in anhydrous benzene, a new set of signals was observed at the ^{1}H NMR spectrum; the spectrum pattern suggested the formation of a partially deprotonated Ru complex due to two sets of signals from inequivalent ligands. The ^{31}P{^{1}H} spectrum also exhibited two distinct signals at 106.1 and 106.3 ppm.

We succeeded in obtaining single crystals suitable for XRD studies from which we elucidated the structure of complex **2** (Fig. 3 and Scheme 3). The X-ray structure of **2**, [Ru$_2$(**L*****-H**)$_2$(**L**)$_2$], shows a dimeric geometry with two-fold symmetry in the solid state, in which each five-coordinate ruthenium center shows a slightly distorted square-pyramid configuration (τ_5 = 0.18). Each Ru center remains coordinated to two P,N-chelating naphthyridinone-based ligands, with one ligand deprotonated at the methylene arm (**L*****-H**) and the other ligand deprotonated at the N-atom (**L**). Deprotonation at the methylene arm is also evident from shorter C11–C12 bond length (1.3797(16) Å) at the methine arm in **L*****-H**, as compared to the methylene arm in **L** (C21-C22 bond of 1.4997(17) Å). The fifth coordination site of Ru is occupied by the O-atom of the N-deprotonated ligand **L** that serves as the bridging moiety.

The ligand **L** is characterized by the elongated C28–O2 bond distance of 1.2931(14) Å as compared to a shorter C18–O1 distance of 1.2397(16) Å in **L*****-H** or protonated **L-H** ligand in complex **1** (C–O 1.2291(11)-1.2311(11) Å). This indicates that the resonance structure depicting ligand **L** in **2** as containing an aryloxide-type O$^-$-donor coordinating to a Ru center (as shown in Scheme 3, top) should have a noticeable contribution. However, as the C–O bond distance in **L*****-H** lies between the typical values for single (ca. 1.35 Å) and double (ca. 1.21 Å) C(sp^2)–O bonds, an alternative resonance structure of **L** in complex **2** as a naphthyridonate-type donor with a negative charge residing on an N-atom is also likely to contribute (Scheme 3, bottom). The formation of a relatively uncommon five-coordinate Ru^{II} center is likely due to steric hindrance imposed by the cyclic dimeric structure and the presence of a negatively charged, electron-rich π-donating amide donor of a deprotonated **L*****-H** ligand. Similarly, five-coordinate square pyramidal Ru^{II} complexes are known for pincer-ligated Ru^{II} complexes, in which one of the CH_2 arms is deprotonated, leading to pyridine dearomatization to give a strong amide donor.[26, 38] Interestingly, we also observed intramolecular hydrogen bonds between the O-atom of **L** and the H-atom of **L*****-H** providing a further stabilization of dimer structure.

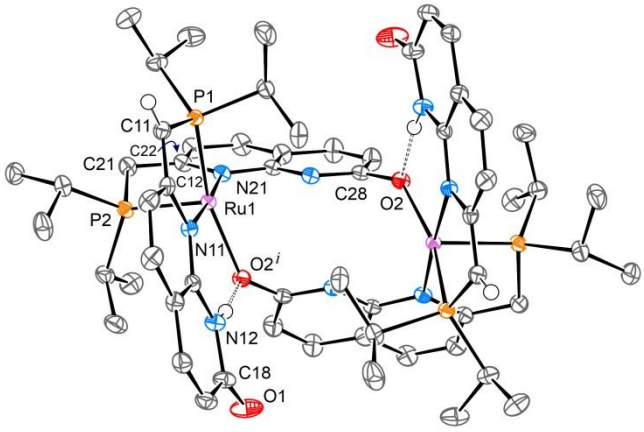

Fig 3 ORTEP of **2** at 60 % probability level according to single crystal X-ray diffraction data. Solvent molecules and hydrogen atoms, except for N–H and deprotonated arms, are omitted for clarity. Selected interatomic distances [Å]: Ru1–N11 2.1765(9), Ru1–N21 2.0646(10), Ru1–O2^i 2.1848(9), Ru1–P1 2.2412(3), Ru1–P2 2.1913(3). H-bond N12–H12···O2^i [Å, °]: N12–H12 0.81(2), H12···O2^i 1.88(2), N12···O2^i 2.6790(13), ∠N12–H12···O2^i 172(2). Equivalent atoms are labeled by the superscript sign *i*: symmetry operation is (1 – *x*, *y*, 3/2 – *z*).

View Article Online
DOI: 10.1039/D0DT02505D

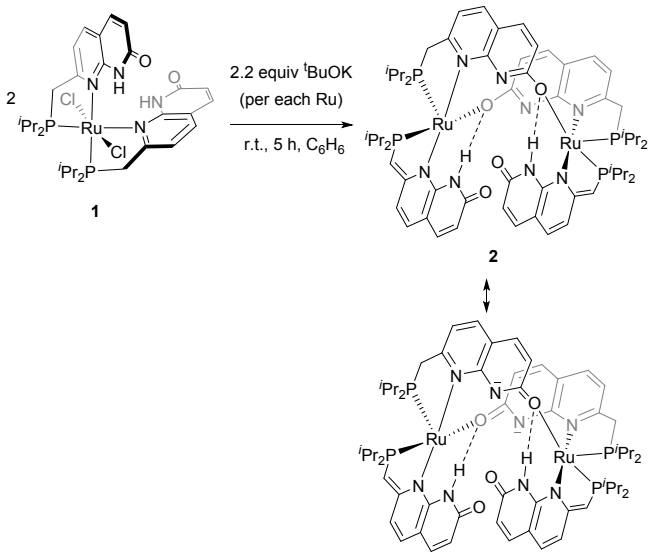

Scheme 3 Deprotonation of complex **1** with ^{t}BuOK yielding complex **2**.

The ^{1}H NMR spectrum in solution was also consistent with the solid-state structure and showed the presence of two inequivalent ligands, one ligand being deprotonated at the N-atom and the other one being deprotonated at the methylene fragment. The multiplets at 2.94 and 2.73 ppm with relative integration as two protons have been assigned as one of the CH_2 groups, while the broad peak integrating as 1H at 4.09 ppm has been assigned to the deprotonated CH-fragment, which overlaps with another peak from CH protons of the naphthyridinone fragment of the ligand. Interestingly, the N–H peak is significantly downfield shifted and appears at 18.09 ppm, which could be due to the persistence of the hydrogen bond that is observed in the solid state.[39] Thus, the dimeric or oligomeric structure likely persists in solutions of non-coordinating solvents. The highly reactive nature of neutral complex **2** did not allow for its characterization by ESI-MS. Isolated complex **2** could be stored in the solid state under an inert atmosphere at –20 °C for several weeks with only minor decomposition; however, it was highly reactive in the presence of protic solvents (vide infra).

Reactivity of 2 with water and alcohols.

Considering that complex **2** contains several basic reactive sites that can be easily protonated, we investigated the reactivity of **2** with water and alcohols. Addition of 5 equiv. of H_2O to a benzene solution of **2** at r.t. promoted instant color change from dark brown to bright yellow accompanied by the precipitation of a solid material. This product could be easily isolated, washed with benzene, and characterized by XRD (Fig. 4), NMR, UV-vis, IR spectroscopies and elemental analysis. According to XRD, the complex can be described as a *cis*-diaqua complex **3** of $Ru(\mathbf{L})_2(OH_2)_2$ composition with both ligands **L** protonated at the methylene arm (Scheme 4). Intramolecular hydrogen bonds are present between the aqua ligands and the deprotonated terminal N-atoms of naphthyridinones; parameters of the H-bonds are given in the caption of Fig 4. Additionally, an intermolecular hydrogen bonded network composed by two complexes and four free, non-coordinating water molecules forms the asymmetric cell in the crystals (see ESI, Figures S46-S47). It should be noted that all O–H and N–H hydrogen atoms for complexes **1**-**4** were found using the difference Fourier maps and refined isotropically. The Ru–N bond length is shorter (ca. 2.16 Å) compared to complex **1** (ca. 2.24 Å) due to weaker *trans* influence of naphthyridine N-donor in a *cis*-diaqua complex.

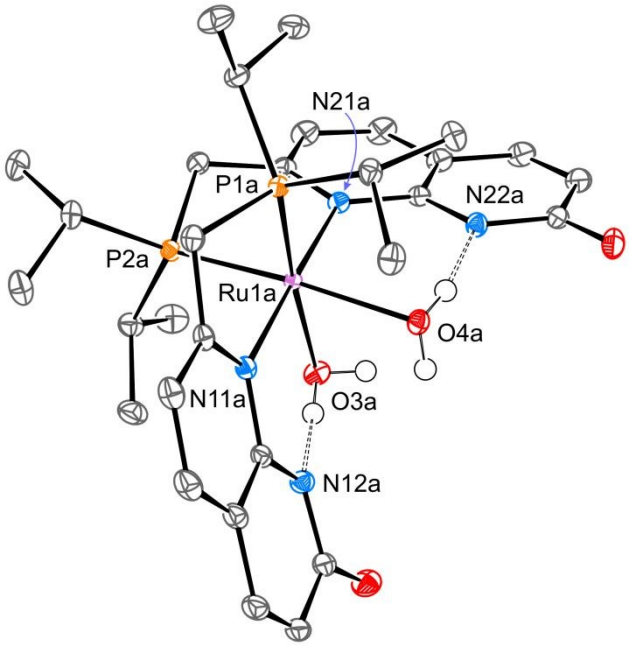

Fig 4 ORTEP of **3** at 60 % probability level according to single crystal X-ray diffraction data. One of two symmetrically independent molecules of complex is shown. Solvent molecules and hydrogen atoms, except for O–H, are omitted for clarity. Selected interatomic distances [Å]: Ru1A–N11A 2.1476(8), Ru1A–N21A 2.1733(8), Ru1A–O3A 2.2211(7), Ru1A–O4A 2.1901(7), Ru1A–P1A 2.2455(3), Ru1A–P2A 2.2598(3). H-bond O3a–H3a1···N12a [Å, °]: O3a–H3a1 0.838(13), H3a1···N12a 1.752(13), O3a···N12a 2.5721(11), ∠O3a–H3a1···N12a 166(2). H-bond O4a–H4a1···N22a [Å, °]: O4a–H4a1 0.833(12), H4a1···N22a 1.739(13), O4a···N22a 2.5545(11), ∠O4a–H4a1···N22a 165.7(19).

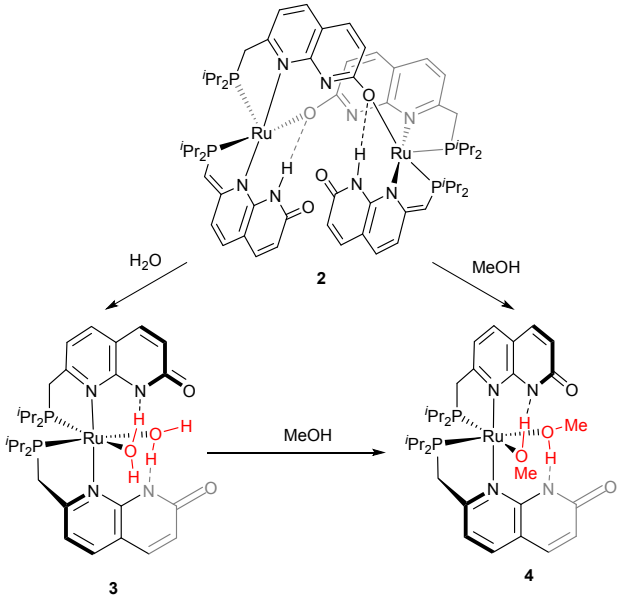

View Article Online
DOI: 10.1039/D0DT02505D

Scheme 4 Reactivity of complex **2** with protic solvents.

Complex **3** exhibits low solubility in most non-protic solvents, it was also very sparingly soluble in water, which prevented us from obtaining its full NMR characterization. When complex **3** was dissolved in $CDCl_3$ or CD_2Cl_2, the solution color slowly changed from yellow to orange leading to the formation of chloro-complex **1** identified by ^1H NMR. The DFT-optimized geometry of complex **3** shows that the structure is consistent with X-ray analysis, with two aqua ligands attached to the Ru center, H-bonded to negatively charged N-atoms of terminal naphthyridinonates.

Thus, the reaction of dimeric complex **2** with water leads to the protonation of the methylene arm in both ligands **L*-H**, while the *cis*-arrangement of two chelating ligands around the metal center is retained. Interestingly, while complex **2** contains NH groups, its reaction with water leads to their deprotonation, likely by the hydroxide formed after protonation of the methyne CH arm with water.

When complex **3** was dissolved in MeOH, instantaneous water–methanol exchange occurred, generating the new complex Ru(**L**)$_2$(MeOH)$_2$ (**4**). Alternatively, complex **4** can be obtained by dissolving complex **2** in MeOH (Scheme 4). The ^1H NMR in CD_3OD exhibited a symmetrical pattern in which all methylene groups at the chelating ligands are protonated. The $^{31}P\{^1H\}$ NMR spectrum shows a singlet at 74.90 ppm. The higher solubility of the new complex in deuterated solutions allowed us to assign the signals of the methylene fragments, which appear as two doublets of doublets at 3.97 ppm and 3.30 ppm due to coupling to a geminal proton and a phosphorus atom. Since the ^1H NMR was recorded in CD_3OD, fast H/D exchange prevented us from observing the N–H signal by NMR analysis. The new complex was easily crystallized from a concentrated MeOH solution at –20 °C and its single crystal XRD analysis confirmed its monomer structure and similarity to **3**. The MeOH ligands are hydrogen-bonded to deprotonated terminal N-atoms of naphthyridinones similar to complex **3**, as shown in Fig 5.

Although in the solid state the structures of **3** and **4** are described as bis-solvento complexes, in solution proton transfer from neutral water or MeOH ligands to the basic terminal N-atom of naphthyridonate cannot be excluded, or both forms can be present in equilibrium. Both product complexes still retain two basic sites as the negatively charged terminal N-atoms of naphthyridonate, that can potentially participate in SCS reactivity.

Next, we set out to study if complex **3** is active in dehydrogenative transformations of alcohols to aldehydes. A number of Ru and Ir-based complexes have been reported to catalyze dehydrogenation of alcohols to aldehydes,[40-41] and among these systems, utilization of proton-responsive ligands has been demonstrated as a successful strategy to achieve selective transformations via cooperative catalysis.[42-44]

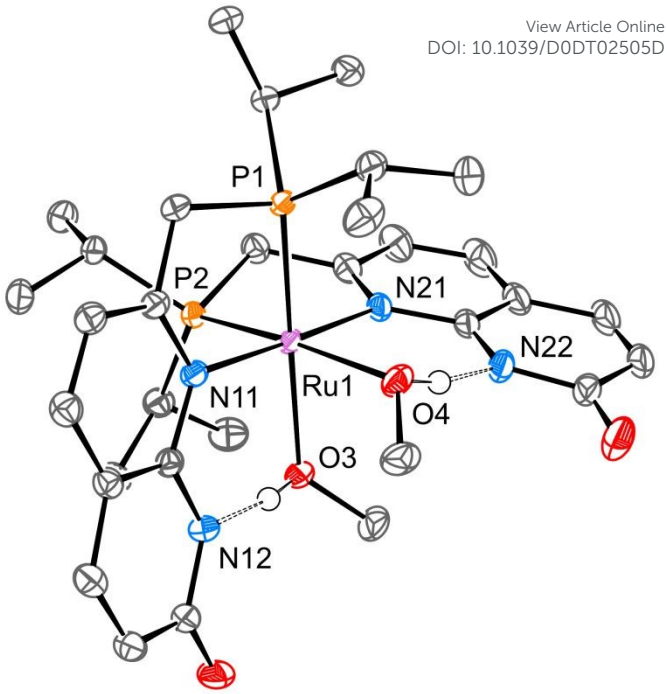

Fig 5 ORTEP of **4** at 60 % probability level according to single crystal X-ray diffraction data. Solvent molecules and hydrogen atoms, except for O–H, are omitted for clarity. Selected interatomic distances [Å]: Ru1–N11 2.1778(11), Ru1–N21 2.1718(12), Ru1–O3 2.1784(10), Ru1–O4 2.2004(10), Ru1–P1 2.2648(3), Ru1–P2 2.2534(3). H-bond O3–H3···N12 [Å, °]: O3–H3 0.872(15), H3···N12 1.639(15), O3···N12 2.5022(16), ∠O3–H3···N12 170(3). H-bond O4–H4···N22 [Å, °]: O4–H4 0.902(15), H4···N22 1.629(16), O4···N22 2.5184(17), ∠O4–H4···N22 168(3).

Acceptorless dehydrogenation of alcohols leading to the formation of hydrogen gas as a byproduct ultimately provides a clean method of producing carbonyls, by contrast to other commonly used oxidative methods that typically produce large amount of hazardous waste.[45] However, due to unfavorable thermodynamics of dehydrogenation of primary alcohols to aldehydes, this transformation still remains challenging.[46] Moreover, base additives often used to activate precious metal catalysts may also lead to side reactions with aldehydes, leading to decreased selectivity towards the desired aldehyde product.[47] Ru complexes that exhibit metal-ligand cooperativity are typically known to transform alcohols directly to esters,[25, 48] and some Ru[20, 49] and other transition metal complexes are very active catalysts for the dimerization of aldehydes to esters.[50-51] Selective and mild catalytic acceptorless dehydrogenation methods that stop at the aldehyde remain sought after.

We used *para*-anisyl alcohol as a model substrate due to the simplicity of the NMR spectra of both product and starting material facilitating quantitative NMR analysis. Using 5 mol% of **3** in the presence of *para*-anisyl alcohol in a refluxing toluene solution, the corresponding aldehyde was obtained as the only product in 43% yield after 16 h at 110 °C. Considering that primary alcohol dehydrogenation to aldehyde is thermodynamically endergonic and endothermic, typically high temperature and efficient removal of H_2 product is required to drive the reaction forward. Accordingly, when the

Published on 28 August 2020.

View Article Online DOI: 10.1039/D0DT02505D

reaction was performed in *para*-xylene at 160 °C, higher yields and conversions were obtained, although long reaction time was still required to reach the 88% yield of aldehyde after 72 h (Scheme 5).

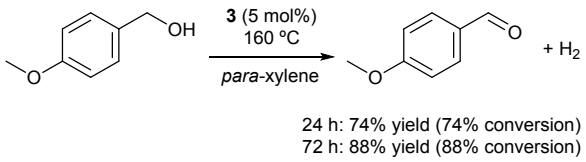

Scheme 5. Dehydrogenation of *para*-anisyl alcohol catalyzed by **3**.

Considering that other catalytic systems showing reversible alcohol dehydrogenation have been utilized in the deuteration of alcohols in α- and β-positions using D_2O as a source in the presence of a Ru complex and catalytic base, we also examined the reactivity of complex **3** with alcohols in neat D_2O in a closed system.[52] Under these conditions, partial deuteration of *para*-anisyl alcohol was observed in the α-position (Scheme 6). In the case of 1-hexanol, partial deuteration was observed in both α- and β-positions, in a latter case, likely via keto-enol tautomerism.[52]

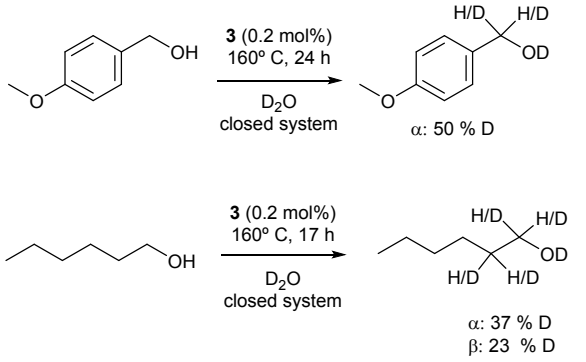

Scheme 6. Deuteration of alcohols in neat D_2O catalyzed by **3**.

Based on the reactivity studies described above and considering that dissociation of aqua or MeOH ligands in complexes **3** or **4** may provide potentially two coordination sites in the *cis*-position to each other, we propose an inner sphere mechanism, in which basic sites at the N-atoms of the naphthyridonates play a role in the deprotonation of an alcohol and assist in the formation of H_2 gas (Scheme 7). A DFT computational study to examine a possible mechanism for **3**-catalyzed dehydrogenation of alcohols to aldehydes was done using B3LYP functional and LANL2DZ (for Ru)/6–31G+(d,p) (for non-metal atoms) basis sets; benzyl alcohol was chosen as a model system to avoid differences associated with different orientation of OMe group. The net reaction, dehydrogenation of benzyl alcohol to benzaldehyde and H_2, was estimated to be endergonic and endothermic, with ΔG and ΔH values of 2.1 kcal mol^{-1} and 9.7 kcal mol^{-1}, respectively. In the proposed pathway, displacement of water with benzyl alcohol leads to the formation of an intermediate **A**, in which short hydrogen bonding is observed between terminal N-atom of naphthyridonate and OH group of the alcohol, and a pentacoordinate Ru atom has a square pyramidal geometry. Attempts to optimize a Ru^{II} complex bearing benzyl alkoxide with the N-atom protonated, **L–H**, always yielded intermediate **A**. Due to the presence of a *cis*-vacant coordination site, subsequent β-hydride elimination via **TS-AB** produces a Ru hydride complex **B** with an aldehyde coordinated to Ru center. This step is endothermic with respect to **A** by 25.35 kcal·mol^{-1} and is characterized by an activation barrier of 26.35 kcal mol^{-1}. Substitution of benzaldehyde by benzyl alcohol to generate intermediate **C** is exothermic by 25.1 kcal mol^{-1}. Release of H_2 regenerates intermediate **A** through the transition state **TS-CA**, with an activation barrier of 17.91 kcal mol^{-1}. In the H_2 liberation step, the proton is provided by the NH group of the protonated naphthyridinone fragment.

Overall, although benzylic alcohols can be dehydrogenated to aldehydes under acceptor-free and base-free conditions using complex **3**, sluggish reactivity makes this system much less competitive compared to existing catalysts,[41-44, 46, 53] leading us to conclude that the naphthyridinone-based ligand motif may not be well-suited to the promotion of such transformations.

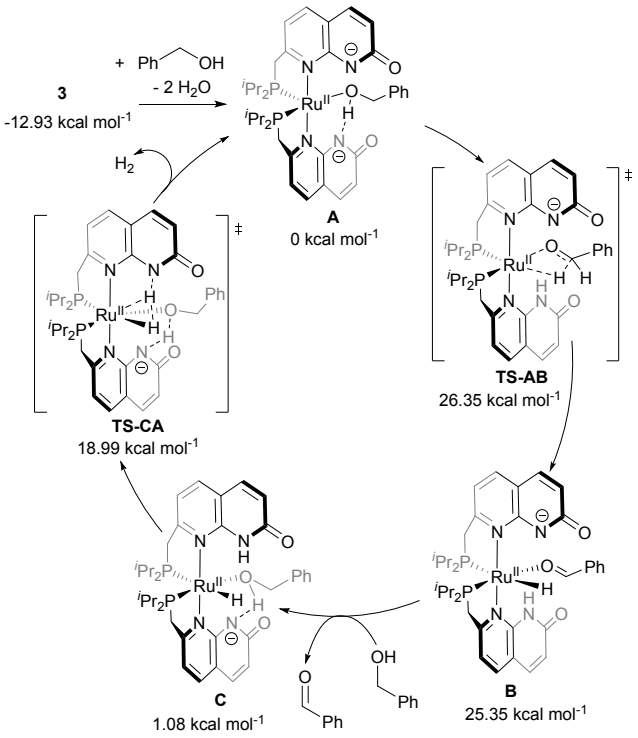

Scheme 7. Proposed mechanism for Ru-catalyzed dehydrogenation of alcohols to aldehydes.

Conclusions

Herein we described the synthesis, characterization, and reactivity for a new family of Ru^{II} complexes bearing a naphthyridinone-based ligand with proton responsive groups in the secondary coordination sphere. We obtained the doubly deprotonated dimeric complex **2** with two pairs of ligands

displaying both possible deprotonation modes: with one pair of ligands deprotonated at the N-atom (**L**) and the other at the methylene arm (**L*-H**), retaining its terminal NH groups. The second type ligands also featuring short hydrogen bonds at the NH to the oxygen atom of the first type ligand (**L**). Complex **2** proved to be highly unstable in non-hydrocarbon solvents. We also studied the reactivity of **2** with protic solvents and isolated complexes **3** and **4**, which contain two aqua or two MeOH ligands. Furthermore, complexes **2**-**4** promote oxidant-free dehydrogenation of *para*-anisyl alcohol to the corresponding aldehyde in the absence of a base or extra additives; however, the reactivity is rather moderate and requires forcing conditions. Overall, the main interest towards further study of such ligand systems in small molecule activation stems from the observation of a ditopic reactivity in deprotonation as well as the formation of bis-solvato complexes with two internal proton shuttle sites that may promote other types of hydrogen or proton transfer reactions. The current study proved the basic viability of this concept. We plan to further study the potential application of these ligands in cooperative bond activation via participation of the ligand as an internal base with metals other than ruthenium.

Experimental

General specifications

All operations were carried out under an atmosphere of argon or nitrogen using standard Schlenk and glove box techniques. Anhydrous deuterated solvents were acquired from Eurisotop and stored over 4 Å molecular sieves. Anhydrous solvents were obtained using an MBRAUN solvent purification system and degassed prior to use. NMR spectra were measured on JEOL ECZ600R 600MHz, JEOL ECZ400S 400 MHz and Bruker Avance II 400 MHz spectrometers. The following abbreviations are used for describing NMR spectra: s (singlet), d (doublet), t (triplet), m (multiplet), br (broad), q (quaternary). Electrospray ionization mass spectrometry (ESI-MS) measurements were performed on a Thermo Scientific ETD apparatus. Elemental analyses were completed using an Exeter Analytical CE440 instrument. FT-IR spectra were measured using an Agilent Cary 630 spectrometer equipped with an ATR module in an argon filled glovebox. The following abbreviations are used for describing FT-IR spectra: s (strong), m (medium), w (weak), br (broad). UV/vis spectra were collected using an Agilent Cary 60 spectrophotometer. Literature method was used to prepare Ru precursor $Ru(DMSO)_4Cl_2$[54] and 7-(chloromethyl)-1,8-naphthyridin-2(1*H*)-one (*ClNaph*) precursor.[33]

Synthesis of ligand L-H. 3 g of chloride precursor *ClNaph* (15.43 mmol) was added to a solution of 2.19 g of $^{i}Pr_2PH$ (18.5 mmol) in methanol. Resulting solution was heated at 80 °C for 18 hours with magnetic stirring. After the solution was cooled to room temperature, 2.6 mg of $NaHCO_3$ (31 mmol) was slowly added (to avoid violent effervescence) while stirring the solution. Then the solvents and volatiles were removed under vacuum. A mixture of CH_2Cl_2 (DCM) and water was added (1:20 v/v water : DCM) and the solution was stirred for 15 minutes. The ligand was extracted in DCM and dried over $MgSO_4$. The crude ligand was purified by washing with water. An off-white solid is isolated and dried under vacuum (2.7 g, 63% yield). ^{1}H NMR (400 MHz, CD_3CN): δ 10.24 (s, 1H, NH_{Naph}), 7.83 (d, *J* = 7.9 Hz, 1H, CH_{Naph}), 7.73 (d, *J* = 9.5 Hz, 1H, CH_{Naph}), 7.13 (d, *J* = 7.9 Hz, 1H, CH_{Naph}), 6.47 (d, *J* = 9.5 Hz, 1H, CH_{Naph}), 3.00 (d, J_{HP} = 1.9 Hz, 2H, CH_2), 1.87-1.61 (m, 2H, CH_{iPr}), 1.12-0.84 (m, 12H, CH_{3iPr}). $^{13}C\{^1H\}$ NMR (101 MHz, CD_3CN): δ 163.57 (d, J_{CP} = 8.6 Hz, C_q, C=O), 163.20 (C_q, C_{Naph}), 149.36 (C_q, C_{Naph}), 139.18 (CH, C_{Naph}), 136.36 (CH, C_{Naph}), 121.70 (CH, C_{Naph}), 118.82 (d, J_{CP} = 6.0 Hz, CH, C_{Naph}), 112.15 (C_q, C_{Naph}), 32.41 (d, J_{CP} = 23.7 Hz, CH_2–P), 23.48 (d, J_{CP} = 15.0 Hz, CH, C_{iPr}), 19.10 (d, J_{CP} = 15.3 Hz ,CH_3, C_{iPr}), 18.36 (d, J_{CP} = 10.7 Hz CH_3, C_{iPr}). $^{31}P\{^1H\}$ NMR (243 MHz, CD_3CN): δ 15.48 (s). UV/vis (CH_3OH), λ, nm (ε, M^{-1} cm^{-1}): 212 (63500), 262 (6550), 330 (35100), 344 (26910). FT-IR (ATR, solid, cm^{-1}): ν, 3053 (br), 1647 (s), 1568 (s), 1539 (m), 1495(m).

Synthesis of complex 1, $Ru(L\text{-}H)_2Cl_2$. A solution of 1 g (3.620 mmol) of **L-H** and 0.85 g (1.75 mmol) of $Ru(DMSO)_4Cl_2$ in 25 mL of THF were heated and stirred at 80 °C for 8 hours in a 100 mL Schlenk tube. The initially yellow suspension changed color to deep orange. Once the solution was cooled to r.t., diethyl ether was added (25 mL) generating an orange solid that was filtered and washed with diethyl ether (2 x 25 mL) to remove the excess of ligand. An orange solid was isolated (1.22 g, 96% yield). The orange solid was recrystallized from a saturated solution in THF, filtered and stored at –20 °C under an inert atmosphere to give crystals suitable for X-ray diffraction study. ^{1}H NMR (400 MHz, CD_2Cl_2): δ 11.32 (s, 2H, NH_{Naph}), 7.87 (d, *J* = 7.9 Hz, 2H, CH_{Naph}), 7.54 (d, *J* = 9.4 Hz, 2H, CH_{Naph}), 7.43 (d, *J* = 7.9 Hz, 2H, CH_{Naph}), 6.27 (dd, *J* = 9.4, 1.9 Hz, 2H, CH_{Naph}), 4.70 (dd, *J* = 16.8, 6.9 Hz, 2H, CH_2), 3.58 (dd, *J* = 16.8, 12.4 Hz, 2H, CH_2), 2.72 (m, 2H, CH_{iPr}), 2.50 (m, 2H, CH_{iPr}), 1.44 (m, 12H, $CH_{3,iPr}$), 1.15 (m, 6H, $CH_{3,iPr}$), 0.99 (m, 6H, $CH_{3,iPr}$). ^{1}H NMR (400 MHz, $CDCl_3$): δ 11.33 (s, 2H, NH_{Naph}), 7.89 (d, *J* = 8.0 Hz, 2H, CH_{Naph}), 7.56 (d, *J* = 9.5 Hz, 2H, CH_{Naph}), 7.45 (d, *J* = 8.0 Hz, 2H, CH_{Naph}), 6.28 (dd, *J* = 9.5, 1.9 Hz, 2H, CH_{Naph}), 4.72 (dd, *J* = 17.0, 7.1 Hz, 2H, CH_2), 3.58 (dd, *J* = 17.0, 12.4 Hz, 2H, CH_2), 2.73 (m, 2H, CH_{iPr}), 2.53 (m, 2H, CH_{iPr}), 1.46 (m, 12H, $CH_{3,iPr}$), 1.13 (m, 6H, $CH_{3,iPr}$), 1.01 (m, 6H, $CH_{3,iPr}$). $^{13}C\{^1H\}$ NMR (101 MHz, $CDCl_3$): δ 165.74 (C_q, C=O), 161.06 (C_q, C_{Naph}), 152.90 (C_q, C_{Naph}), 138.48 (CH, C_{Naph}), 137.35 (CH, C_{Naph}), 122.13 (CH, C_{Naph}), 118.09 (CH, C_{Naph}), 113.51 (C_q, C_{Naph}), 38.37 (m, CH_2–P), 27.35 (m, CH, C_{iPr}), 26.91 (m, CH, C_{iPr}), 20.60 (CH_3, C_{iPr}), 19.35 (CH_3, C_{iPr}), 19.00 (CH_3, C_{iPr}), 18.77 (CH_3, C_{iPr}). $^{31}P\{^1H\}$ NMR (243 MHz, $CDCl_3$): δ 70.29 (s). Elemental analysis: Calcd. For $C_{30}H_{42}Cl_2N_4O_2P_2Ru$: C, 49.73; H, 5.84; N, 7.73. Found: C, 49.65; H, 6.24; N, 7.49. UV/vis (CH_3CN), λ, nm (ε, M^{-1} cm^{-1}): 228 (80700), 249 (35900), 330 (29800), 341 (26300). FT-IR (ATR, solid, cm^{-1}): ν, 3137 (br), 1663 (s), 1595 (s), 1544 (w), 1457 (w).

Synthesis of complex 2 $[Ru_2(L^*\text{-}H)_2(L)_2]$. In a 20 mL vial, 100 mg of complex **1** (0.138 mmol) and 17.3 mg of potassium *tert*-butoxide (0.303 mmol) were suspended in 15 mL of toluene. The resulting brown suspension was magnetically stirred for 5 hours at r.t.. Then volatiles and solvents were evaporated under vacuum. After this, the resulting solids were dissolves in benzene and the mixture was filtered to remove inorganic salts, giving rise to a brown solution, which was evaporated

View Article Online
DOI: 10.1039/D0DT02585D

View Article Online DOI: 10.1039/D0DT02505D

under vacuum. 117 mg of deep brown solid was isolated; yield 65%. Crystals suitable for X-ray diffraction were obtained from a concentrated solution in benzene. Satisfactory elemental analysis could not be obtained even after multiple attempts of recrystallization due to low stability.

When complex **1** was reacted with excess base (10 equiv of ^{t}BuOK in THF-d_8), the formation of a mixture of unidentified products was observed.

^{1}H NMR (400 MHz, C_6D_6): δ 18.09 (s, 2H, NH_{Naph}), 6.99 (d, *J* = 7.8 Hz, 2H, CH_{Naph}), 6.89 (d, *J* = 8.9 Hz, 2H, CH_{Naph}), 6.55 (d, *J* = 8.7 Hz, 2H, CH_{Naph}), 6.49 (d, *J* = 7.9 Hz, 2H, CH_{Naph}), 6.44 (d, *J* = 7.8 Hz, 2H, CH_{Naph}), 6.40 (br s, 2H, CH_{Naph}), 6.32 (d, *J* = 8.6 Hz, 2H, CH_{Naph}), 4.02 (br s, 4H, overlapped CH_{Naph} and =CHP), 2.85 (dd, *J* = 17.8, 10.6 Hz, 2H, CH_2), 2.64 (dd, *J* = 17.8, 7.6 Hz, 2H, CH_2), 2.39-2.20 (m, 2H, CH_{iPr}), 2.19-1.98 (m, 4H, CH_{iPr}), 1.54-1.37 (m, 8H, $CH_{3,iPr}$ overlapping with CH_{iPr}), 1.20 (dd, *J* = 14.8, 6.8 Hz, 6H, $CH_{3,iPr}$), 1.11 (dd, *J* = 14.2 Hz, 7.0 Hz, 6H, $CH_{3,iPr}$), 1.02-0.86 (m, 12H, $CH_{3,iPr}$), 0.85-0.70 (m, 12H, $CH_{3,iPr}$), 0.26 (dd, *J* = 14.2, 7.2 Hz, 6H, $CH_{3,iPr}$). ^{13}C{^{1}H} NMR (101 MHz, C_6D_6): δ 173.28 (C_q, C=O), 164.12 (C_q, C_{Naph}), 159.20 (d, J_{CP} = 3.4 Hz, C_q, C_{Naph}), 133.11 (CH, C_{Naph}), 130.35 (C_q, C_{Naph}), 129.00 (C_q, C_{Naph}), 126.24 (CH, C_{Naph}), 114.73 (CH, C_{Naph}), 114.61 (CH, C_{Naph}), 113.07 (C_q, C_{Naph}), 110.13 (CH, C_{Naph}), 110.01 (CH, C_{Naph}), 103.94 (br, CH–P), 37.46 (d, CH_2–P), 28.85 (CH, C_{iPr}), 28.28 (CH_3, C_{iPr}), 26.68 (CH, C_{iPr}), 19.6-16.94 (CH_3, C_{iPr}). Some of the aromatic ^{13}C peaks were not detected either due to overlap or limited solubility; the position of the broad peak at 103.94 ppm was confirmed by a ^{1}H-^{13}C HMQC experiment. ^{31}P{^{1}H} NMR (243 MHz, C_6D_6): δ 106.26 (s), 106.09 (s). UV/vis (C_6H_6), λ, nm (ε, M^{-1} cm^{-1}): 213 (59800), 226 (45800), 372 (11900), 347 (14200), 405 (10500). FT-IR (ATR, solid, cm^{-1}): ν, 1614 (s), 1541 (m), 1498 (s), 1415 (m), 1380 (m).

Complex 3, $Ru(L)_2(OH_2)_2$. 50 mg of complex **2** (0.077 mmol) were dissolved in 5 mL of toluene in a 20 mL vial, to which 7 µL of water (0.4 mmol) was added at r.t. After 1 hour, a yellow precipitate appeared which was filtered and washed with toluene (4 x 5 mL). 45 mg of yellow solid was isolated (85% yield). Crystals for X-ray diffraction study were obtained from a concentrated toluene solution stored at –20 °C for 24 hours. ^{1}H NMR (400 MHz, D_2O): δ 7.86 (d, *J* = 8.0 Hz, 2H, CH_{Naph}), 7.79 (d, *J* = 8.8 Hz, 2H, CH_{Naph}), 7.26 (d, *J* = 8.0 Hz, 2H, CH_{Naph}), 6.58 (d, *J* = 8.8 Hz, 2H, CH_{Naph}), 3.90 (m, 2H, CH_2), 3.31 (m, 2H, CH_2), 2.33 (m, 2H, CH_{iPr}), 2.07 (m, 2H, CH_{iPr}), 1.05 (m, 6H, $CH_{3,iPr}$), 0.94 (m, 6H, $CH_{3,iPr}$), 0.87 (m, 6H, $CH_{3,iPr}$), 0.54 (m, 6H, $CH_{3,iPr}$). Elemental analysis: Calcd. For $C_{30}H_{48}N_4O_6P_2Ru$: C, 49.79; H, 6.69; N, 7.74. Found: C, 49.32; H, 5.99; N, 7.61. UV/vis (C_6H_6), λ, nm (ε, M^{-1} cm^{-1}): 213 (59800), 226 (45800), 372 (11900), 347 (14200), 405 (10500). FT-IR (ATR, solid, cm^{-1}): ν, 3214 (br), 1623 (s), 1544 (s), 1495 (m), 1395 (s).

Complex 4, $Ru(L)_2(MeOH)_2$. 15 mL of methanol was added to 50 mg (0.077 mmol) of complex **3,** immediately generating a yellow solution. After removing the solvent under vacuum, 51 mg of a yellow solid was isolated (91% yield). A concentrated solution in methanol stored at –20 °C under an N_2 atmosphere for 24 hours gave yellow crystals suitable for X-ray diffraction study. Complex **4** can alternatively be obtained by dissolving complex **2** in methanol. However, this synthetic approach gives lower yield after the purification process. ^{1}H NMR (400 MHz, CD_3OD): δ 7.92 (d, *J* = 7.9 Hz, 2H, CH_{Naph}), 7.78 (d, *J* = 9.0 Hz, 2H, CH_{Naph}), 7.31 (d, *J* = 7.9 Hz, 2H, CH_{Naph}), 6.65 (d, *J* = 9.0 Hz, 2H, CH_{Naph}), 4.05-3.90 (m, 2H, CH_2), 3.37-3.25 (m, 2H, CH_2; overlapped with solvent peak), 2.52 (m, 2H, CH_{iPr}), 2.14 (m, 2H, CH_{iPr}), 1.32-1.10 (m, 12H, $CH_{3,iPr}$), 1.00 (m, 6H, $CH_{3,iPr}$), 0.71 (m, 6H, $CH_{3,iPr}$). ^{13}C{^{1}H} NMR (101 MHz, CD_3OD): δ 171.46 (C_q, C=O), 167.54 (C_q, C_{Naph}), 162.27 (C_q, C_{Naph}), 138.08 (CH, C_{Naph}), 136.94 (CH, C_{Naph}), 121.14 (CH, C_{Naph}), 115.35 (CH, C_{Naph}), 114.90(C_q, C_{Naph}), 40.10 (d, J_{CP} = 23.1 Hz, CH_2–P), 29.49 (m, CH, C_{iPr}), 24.55 (m, CH, C_{iPr}), 18.73 (CH_3, C_{iPr}), 17.91 (CH_3, C_{iPr}), 17.56 (CH_3, C_{iPr}), 14.10 (CH_3, C_{iPr}). ^{31}P{^{1}H} NMR (243 MHz, CD_3OD): δ 74.90 (d). Elemental analysis: Calcd. For $C_{32}H_{49}N_4O_4P_2Ru$: C, 53.70; H, 6.76; N, 7.83. Found: C, 53.90; H, 6.78; N, 7.23. UV/vis (CH_3OH), λ, nm (ε, M^{-1} cm^{-1}): 213 (119000), 223 (128500), 277 (42900), 345 (63800), 372 (42600). FT-IR (ATR, solid, cm^{-1}): ν, 3334 (br), 1619 (m), 1550 (s), 1416 (s).

Acceptorless, base-free *p*-anisyl alcohol dehydrogenation to aldehyde (Scheme 5). *Cation! Due to evolution of H_2, the reaction must be performed in an open system equipped with an efficient condenser under a constant stream of inert gas, away from open flame or ignition sources!* All the described dehydrogenation reactions were carried out following the same procedure, varying the temperature, time and solvent as appropriate. Under an inert atmosphere, 3 mL of solvent was added to a 100 mL Schlenk flask. Then 0.22 mmol of alcohol, 0.22 mmol of mesitylene (internal standard) and the 5 mol% of catalyst **3** were dissolved in the solvent. The resulting yellow solution was stirred vigorously using a magnetic stirring bar and heated in an oil bath at constant temperature. A constant stream of N_2 was introduced into the system through the adapter connected to the condenser during the reaction to effectively remove H_2 gas. After the indicated reaction time, the solution was cooled to r.t. for 30 minutes. The conversion of alcohol to the corresponding aldehyde and the yield of aldehyde were calculated by ^{1}H NMR by comparing the integration of the alcohol and aldehyde signals with those of the internal standard.

Catalytic activity of complex 3 in D_2O (Scheme 6). *Caution! Thick wall high pressure tube must be used to perform the reaction in a closed system at high temperature! The reaction vessel must be protected by a safety shield during heating and it should be cooled down to room temperature before opening the vessel!* Under N_2 atmosphere, 2.5 mL (139.0 mmol) of D_2O was placed into a 100 mL Schlenk flask followed by addition of 4 mmol of alcohol and 0.2 mol% of complex **3**. The Schlenk flask was Teflon-sealed and heated in an oil bath. After heating, the reaction vessel was cooled down to r.t. before opening, and an aliquot is taken from the solution at r.t. and analyzed by ^{1}H NMR.

Crystal structure determination

The X-ray diffraction data for the single crystals **1**-**4** were collected on a Rigaku XtaLab PRO instrument in an ω-scan mode with a PILATUS3 R 200K hybrid pixel array detector and a MicroMax™-003 microfocus X-ray tube using Mo*Kα* (0.71073 Å) radiation at low temperature. Images were

View Article Online
DOI: 10.1039/D0DT02505D

indexed and integrated using the *CrysAlis*^{Pro} (version 1.171.39.20a) data reduction package. Data were corrected for systematic errors and absorption using the *ABSPACK* module: Numerical absorption correction based on Gaussian integration over a multifaceted crystal model and empirical absorption correction based on spherical harmonics according to the point group symmetry using equivalent reflections. The *GRAL* module was used for the analysis of systematic absences and space-group determination. All structures were solved by the direct methods using *SHELXT*-2018/2[55] and refined by the full-matrix least-squares on F^2 using *SHELXL*-2018/3.[56] Non-hydrogen atoms were refined anisotropically, except for the atoms of the disordered benzene molecule in crystal **1**, which were left isotropic. The hydrogen atoms were inserted at the calculated positions and refined as riding atoms, except for the hydrogen atoms at the deprotonated arms and N- and O-atoms (for main disorder component), which were found using the difference Fourier maps and restrained on the similarity if possible. The positions of the hydrogen atoms of methyl groups were found using rotating group refinement with idealized tetrahedral angles. The disorder, if present, was resolved using free variables and reasonable restraints on geometry and anisotropic displacement parameters.

*Crystallographic data for **1**.*

$C_{30}H_{42}Cl_2N_4O_2P_2Ru \times 1.5\ C_6H_6$, orange prism (0.256 × 0.166 × 0.098 mm^3), formula weight 841.74; monoclinic, $P2_1/n$ (No. 14), a = 14.65544(11) Å, b = 16.40142(13) Å, c = 16.48977(14) Å, β = 94.6750(7)°, V = 3950.46(5) Å^3, Z = 4, Z' = 1, T = 93(2) K, d_{calc} = 1.415 g cm^{-3}, μ = 0.652 mm^{-1}, F(000) = 1748; $T_{max/min}$ = 1.000/0.480; 237734 reflections were collected (2.177° ≤ θ ≤ 32.355°, index ranges: –21 ≤ h ≤ 21, –24 ≤ k ≤ 24, –24 ≤ l ≤ 24), 13567 of which were unique, R_{int} = 0.0353, R_σ = 0.0136; completeness to θ of 32.355° 96.0 %. The refinement of 488 parameters with 80 restraints converged to R_1 = 0.0202 and wR_2 = 0.0487 for 12713 reflections with $I > 2\sigma(I)$ and R_1 = 0.0224 and wR_2 = 0.0494 for all data with S = 1.030 and residual electron density, $\rho_{max/min}$ = 0.804 and –0.717 e Å^{-3}. The crystals were grown from a concentrated benzene solution at –20 °C.

*Crystallographic data for **2**.*

$C_{60}H_{80}N_8O_4P_4Ru_2 \times C_6H_6$, orange prism (0.195 × 0.089 × 0.062 mm^3), formula weight 1381.44; monoclinic, $C2/c$ (No. 15), a = 23.71159(19) Å, b = 16.43485(11) Å, c = 16.96510(14) Å, β = 98.7499(8)°, V = 6534.29(9) Å^3, Z = 4, Z' = 1, T = 93(2) K, d_{calc} = 1.404 g cm^{-3}, μ = 0.613 mm^{-1}, F(000) = 2872; $T_{max/min}$ = 1.000/0.745; 149422 reflections were collected (2.429° ≤ θ ≤ 32.107°, index ranges: –35 ≤ h ≤ 34, –24 ≤ k ≤ 24, –25 ≤ l ≤ 24), 10971 of which were unique, R_{int} = 0.0303, R_σ = 0.0119; completeness to θ of 32.107° 95.6 %. The refinement of 396 parameters with 20 restraints converged to R_1 = 0.0237 and wR_2 = 0.0639 for 10150 reflections with $I > 2\sigma(I)$ and R_1 = 0.0264 and wR_2 = 0.0654 for all data with S = 1.045 and residual electron density, $\rho_{max/min}$ = 1.308 and –0.799 e Å^{-3}. The crystals were grown from a concentrated benzene solution at –20 °C.

*Crystallographic data for **3**.*

$C_{30}H_{44}N_4O_4P_2Ru \times 2\ H_2O$, yellow prism (0.294 × 0.238 × 0.213 mm^3), formula weight 723.73; triclinic, $P\bar{1}$ (No. 2), a = 11.47028(6) Å, b = 16.11962(8) Å, c = 17.90744(9) Å, α = 80.8486(4)°, β = 83.2392(4)°, γ = 85.1904(4)°, V = 3238.98(3) Å^3, Z = 4, Z' = 2, T = 94(2) K, d_{calc} = 1.484 g cm^{-3}, μ = 0.631 mm^{-1}, F(000) = 1512; $T_{max/min}$ = 1.000/0.241; 395133 reflections were collected (2.235° ≤ θ ≤ 32.380°, index ranges: –17 ≤ h ≤ 17, –24 ≤ k ≤ 24, –26 ≤ l ≤ 26), 22203 of which were unique, R_{int} = 0.0369, R_σ = 0.0140; completeness to θ of 32.380° 95.7 %. The refinement of 855 parameters with 120 restraints converged to R_1 = 0.0206 and wR_2 = 0.0512 for 20928 reflections with $I > 2\sigma(I)$ and R_1 = 0.0226 and wR_2 = 0.0518 for all data with S = 1.050 and residual electron density, $\rho_{max/min}$ = 0.756 and –0.689 e Å^{-3}. The crystals were from a concentrated aqueous toluene solution at –20 °C.

*Crystallographic data for **4**.*

$C_{32}H_{48}N_4O_4P_2Ru \times 4.732\ CH_4O$, yellow prism (0.146 × 0.079 × 0.062 mm^3), formula weight 867.39; monoclinic, $P2_1/n$ (No. 14), a = 11.71671(13) Å, b = 13.94222(15) Å, c = 25.5940(3) Å, β = 94.7465(10)°, V = 4166.61(8) Å^3, Z = 4, Z' = 1, T = 99(2) K, d_{calc} = 1.383 g cm^{-3}, μ = 0.508 mm^{-1}, F(000) = 1837; $T_{max/min}$ = 1.000/0.713; 223268 reflections were collected (2.275° ≤ θ ≤ 32.150°, index ranges: –17 ≤ h ≤ 17, –20 ≤ k ≤ 20, –38 ≤ l ≤ 38), 14635 of which were unique, R_{int} = 0.0567, R_σ = 0.0208; completeness to θ of 32.150° 99.9 %. The refinement of 561 parameters with 105 restraints converged to R_1 = 0.0322 and wR_2 = 0.0785 for 13266 reflections with $I > 2\sigma(I)$ and R_1 = 0.0368 and wR_2 = 0.0803 for all data with S = 1.096 and residual electron density, $\rho_{max/min}$ = 1.080 and –0.940 e Å^{-3}. The crystals were grown from a concentrated methanol solution at –20 °C.

Computational details. DFT calculation was carried out using Gaussian 09 rev. E.01[57] at B3LYP[58-60] level of theory. LANL2DZ[61] and valence-basis sets was used at Ru. For other atoms, 6–31+G (d, p)[62-64] was employed. The structures reported are either minima (NIMAG=0) or transition states (NIMAG=1) on the potential energy surface. The Cartesian coordinates, solvent corrected values, and discussion of the alternative mechanisms are given in the ESI.

Conflicts of interest

There are no conflicts to declare.

Acknowledgements

The authors thank Mr. A. Villar-Briones and Dr. M. Roy (IAS, OIST) for performing HR-MS analysis and acknowledge OIST for funding. O.R.-W. was a JSPS International Research Fellow. This work was supported by JSPS KAKENHI Grant Number 16F16038.

Notes and references

§ These authors contributed equally.

1. J. R. Khusnutdinova and D. Milstein, *Angew. Chem. Int. Ed.*, 2015, **54**, 12236-12273.
2. C. Gunanathan and D. Milstein, *Chem. Rev.*, 2014, **114**, 12024-12087.
3. R. H. Morris, *Acc. Chem. Res.*, 2015, **48**, 1494-1502.
4. P. A. Dub and J. C. Gordon, *Nat. Rev. Chem.*, 2018, **2**, 396-408.
5. S. A. Cook and A. S. Borovik, *Acc. Chem. Res.*, 2015, **48**, 2407-2414.
6. M. Rakowski Dubois and D. L. Dubois, *Acc. Chem. Res.*, 2009, **42**, 1974-1982.
7. L. V. A. Hale and N. K. Szymczak, *ACS Catal.*, 2018, **8**, 6446-6461.
8. C. E. MacBeth, A. P. Golombek, V. G. Young, C. Yang, K. Kuczera, M. P. Hendrich and A. S. Borovik, *Science*, 2000, **289**, 938.
9. M. Harata, K. Jitsukawa, H. Masuda and H. Einaga, *J. Am. Chem. Soc.*, 1994, **116**, 10817-10818.
10. M. Harata, K. Jitsukawa, H. Masuda and H. Einaga, *Chem. Lett.*, 1996, **25**, 813-814.
11. K. Umehara, S. Kuwata and T. Ikariya, *J. Am. Chem. Soc.*, 2013, **135**, 6754-6757.
12. J. B. Geri and N. K. Szymczak, *J. Am. Chem. Soc.*, 2015, **137**, 12808-12814.
13. R. Matheu, M. Z. Ertem, J. Benet-Buchholz, E. Coronado, V. S. Batista, X. Sala and A. Llobet, *J. Am. Chem. Soc.*, 2015, **137**, 10786-10795.
14. R. Zhong, Z. Wei, W. Zhang, S. Liu and Q. Liu, *Chem*, 2019, **5**, 1552-1566.
15. J. F. Hull, Y. Himeda, W.-H. Wang, B. Hashiguchi, R. Periana, D. J. Szalda, J. T. Muckerman and E. Fujita, *Nat. Chem.*, 2012, **4**, 383-388.
16. E. Fujita, J. T. Muckerman and Y. Himeda, *Biochim. Biophys. Acta, Bioenerg.*, 2013, **1827**, 1031-1038.
17. T. Zhang, C. Wang, S. Liu, J.-L. Wang and W. Lin, *J. Am. Chem. Soc.*, 2014, **136**, 273-281.
18. R. Wang, Y. Tang, M. Xu, C. Meng and F. Li, *J. Org. Chem.*, 2018, **83**, 2274-2281.
19. S. Siek, D. B. Burks, D. L. Gerlach, G. Liang, J. M. Tesh, C. R. Thompson, F. Qu, J. E. Shankwitz, R. M. Vasquez, N. Chambers, G. J. Szulczewski, D. B. Grotjahn, C. E. Webster and E. T. Papish, *Organometallics*, 2017, **36**, 1091-1106.
20. N. Menashe and Y. Shvo, *Organometallics*, 1991, **10**, 3885-3891.
21. M. K. Thorson, K. L. Klinkel, J. Wang and T. J. Williams, *Eur. J. Inorg. Chem.*, 2009, **2009**, 295-302.
22. B. L. Conley, M. K. Pennington-Boggio, E. Boz and T. J. Williams, *Chem. Rev.*, 2010, **110**, 2294-2312.
23. S. Kusumoto and K. Nozaki, *Nat. Commun.*, 2015, **6**, 6296.
24. T. Higashi, H. Ando, S. Kusumoto and K. Nozaki, *J. Am. Chem. Soc.*, 2019, **141**, 2247-2250.
25. J. Zhang, G. Leitus, Y. Ben-David and D. Milstein, *J. Am. Chem. Soc.*, 2005, **127**, 10840-10841.
26. J. Zhang, G. Leitus, Y. Ben-David and D. Milstein, *Angew. Chem. Int. Ed.*, 2006, **45**, 1113-1115.
27. S. Pal, S. Kusumoto and K. Nozaki, *Organometallics*, 2018, **37**, 906-914.
28. K.-N. T. Tseng, J. W. Kampf and N. K. Szymczak, *Organometallics*, 2013, **32**, 2046-2049.
29. A. R. Sahoo, F. Jiang, C. Bruneau, G. V. M. Sharma, S. Suresh, T. Roisnel, V. Dorcet and M. Achard, *Catal. Sci. Technol.*, 2017, **7**, 3492-3498.
30. A. R. Sahoo, G. Lalitha, V. Murugesh, C. Bruneau, G. V. M. Sharma, S. Suresh and M. Achard, *J. Org. Chem.*, 2017, **82**, 10727-10731.
31. A. Dubey, L. Nencini, R. R. Fayzullin, C. Nervi and J. R. Khusnutdinova, *ACS Catal.*, 2017, **7**, 3864-3868.
32. A. Dubey, S. M. W. Rahaman, R. R. Fayzullin and J. R. Khusnutdinova, *ChemCatChem*, 2019, **11**, 3844-3852.
33. O. Rivada-Wheelaghan, S. L. Aristizábal, J. López-Serrano, R. R. Fayzullin and J. R. Khusnutdinova, *Angew. Chem. Int. Ed.*, 2017, **56**, 16267-16271.
34. O. Rivada-Wheelaghan, A. Comas-Vives, R. R. Fayzullin, A. Lledós and J. Khusnutdinova, *Chem. Eur. J.*, 2020, DOI: 10.1002/chem.202002013.
35. A. Kumar, P. Daw, N. A. Espinosa-Jalapa, G. Leitus, L. J. W. Shimon, Y. Ben-David and D. Milstein, *Dalton Trans.*, 2019, **48**, 14580-14584.
36. E. Fogler, J. A. Garg, P. Hu, G. Leitus, L. J. W. Shimon and D. Milstein, *Chem. Eur. J.*, 2014, **20**, 15727-15731.
37. S. Y. de Boer, T. J. Korstanje, S. R. La Rooij, R. Kox, J. N. H. Reek and J. I. van der Vlugt, *Organometallics*, 2017, **36**, 1541-1549.
38. J. Bootsma, B. Guo, J. G. de Vries and E. Otten, *Organometallics*, 2020, **39**, 544-555.
39. S. Zhou and L. Wang, *PCCP*, 2020, **22**, 4884-4895.
40. A. Dobson and S. D. Robinson, *Inorg. Chem.*, 1977, **16**, 137-142.
41. A. Prades, E. Peris and M. Albrecht, *Organometallics*, 2011, **30**, 1162-1167.
42. R. Kawahara, K.-i. Fujita and R. Yamaguchi, *Angew. Chem. Int. Ed.*, 2012, **51**, 12790-12794.
43. R. Kawahara, K.-i. Fujita and R. Yamaguchi, *J. Am. Chem. Soc.*, 2012, **134**, 3643-3646.
44. K.-i. Fujita, T. Yoshida, Y. Imori and R. Yamaguchi, *Org. Lett.*, 2011, **13**, 2278-2281.
45. J. March, *Advanced Organic Chemistry: Reactions, Mechanisms, and Structure* Willey, New York, 3 rd edn., 1985.
46. Z. Liu, J. Caner, A. Kudo, H. Naka and S. Saito, *Chem. Eur. J.*, 2013, **19**, 9452-9456.
47. F. A. Carey and R. M. Giuliano, *Organic Chemistry*, McGraw-Hill Professional, 10th edn., 2016.
48. J. Zhang, M. Gandelman, L. J. W. Shimon and D. Milstein, *Dalton Trans.*, 2007, 107-113.
49. D. G. Gusev and D. M. Spasyuk, *ACS Catal.*, 2018, **8**, 6851-6861.
50. S. A. Morris and D. G. Gusev, *Angew. Chem. Int. Ed.*, 2017, **56**, 6228-6231.
51. C. Tejel, M. A. Ciriano and V. Passarelli, *Chem. Eur. J.*, 2011, **17**, 91-95.
52. E. Khaskin and D. Milstein, *ACS Catal.*, 2013, **3**, 448-452.
53. G. Zeng, S. Sakaki, K.-i. Fujita, H. Sano and R. Yamaguchi, *ACS Catal.*, 2014, **4**, 1010-1020.
54. T.B. Rauchfuss (Ed.) (2010). Ruthenium Complexes. In Inorganic Syntheses, pp. 148-163. DOI:10.1002/9780470651568.ch8.
55. G. Sheldrick, *Acta Crystallogr., Sect. A*, 2015, **71**, 3-8.
56. G. Sheldrick, *Acta Crystallogr., Sect. C*, 2015, **71**, 3-8.
57. M. J. Frisch, G. W. Trucks, H. B. Schlegel, G. E. Scuseria, M. A. Robb, J. R. Cheeseman, G. Scalmani, V. Barone, G. A. Petersson, H. Nakatsuji, X. Li, M. Caricato, A. Marenich, J. Bloino, B. G. Janesko, R. Gomperts, B. Mennucci, H. P. Hratchian, J. V. Ortiz, A. F. Izmaylov, J. L. Sonnenberg, D.

View Article Online
DOI: 10.1039/D0DT02505D

Williams-Young, F. Ding, F. Lipparini, F. Egidi, J. Goings, B. Peng, A. Petrone, T. Henderson, D. Ranasinghe, V. G. Zakrzewski, J. Gao, N. Rega, G. Zheng, W. Liang, M. Hada, M. Ehara, K. Toyota, R. Fukuda, J. Hasegawa, M. Ishida, T. Nakajima, Y. Honda, O. Kitao, H. Nakai, T. Vreven, K. Throssell, J. A. Montgomery, Jr., J. E. Peralta, F. Ogliaro, M. Bearpark, J. J. Heyd, E. Brothers, K. N. Kudin, V. N. Staroverov, T. Keith, R. Kobayashi, J. Normand, K. Raghavachari, A. Rendell, J. C. Burant, S. S. Iyengar, J. Tomasi, M. Cossi, J. M. Millam, M. Klene, C. Adamo, R. Cammi, J. W. Ochterski, R. L. Martin, K. Morokuma, O. Farkas, J. B. Foresman, and D. J. Fox, Gaussian 09, Revision E.01. Gaussian, Inc., Wallingford CT, 2013.

58. C. Lee, W. Yang and R. G. Parr, *Phys. Rev. B*, 1988, **37**, 785-789.
59. A. D. Becke, *J. Chem. Phys.*, 1993, **98**, 5648-5652.
60. A. D. Becke, *J. Chem. Phys.*, 1996, **104**, 1040-1046.
61. P. J. Hay and W. R. Wadt, *J. Chem. Phys.*, 1985, **82**, 299-310.
62. T. Clark, J. Chandrasekhar, G. W. Spitznagel and P. V. R. Schleyer, *J. Comput. Chem.*, 1983, **4**, 294-301.
63. M. J. Frisch, J. A. Pople and J. S. Binkley, *J. Chem. Phys.*, 1984, **80**, 3265-3269.
64. R. Krishnan, J. S. Binkley, R. Seeger and J. A. Pople, *J. Chem. Phys.*, 1980, **72**, 650-654.

Published on 28 August 2020.

View Article Online
DOI: 10.1039/D0DT02505D

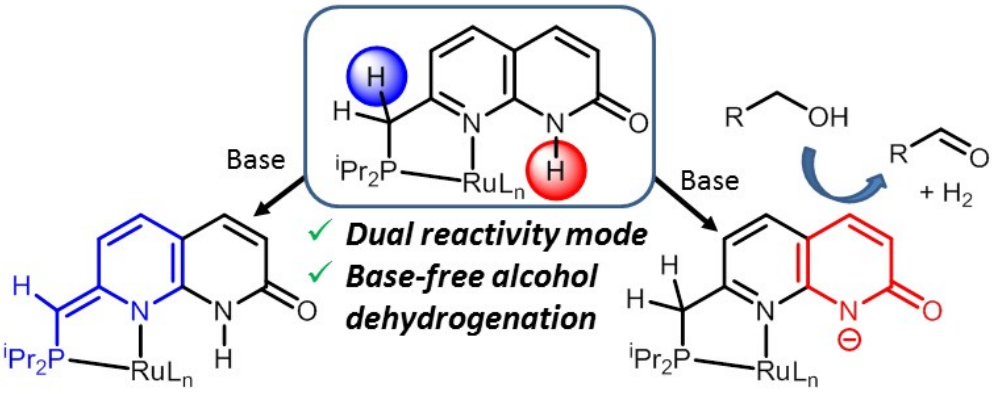

201x82mm (96 x 96 DPI)

Published on 28 August 2020.